Supporting Information

Water envelope has a critical impact in the design of protein-protein interaction inhibitors

Ekaterina L. Ratkova,* Maciej Dawidowski, Valeria Napolitano, Grzegorz Dubin, Roberto Fino, Michael S. Ostertag, Michael Sattler, Grzegorz Popowicz,* and Igor V. Tetko*

Table of Content

1. Methods

1.1. Theoretical methods and computational details

1.1.1. The Reference Interaction Site Model (RISM)

Several computational methods have been developed over the last years for an analysis of explicit water molecules position in a binding pocket. They mainly follow the same workflow (Scheme S1) having the methodological difference at the first step, i.e. estimation of water distribution function. Two general approaches can be applied for this purpose: explicit and implicit solvent methods. Here, we employed

the Reference Interaction Site Model (RISM)[1] approximation of the Integral Equation Theory (IET) – a class of implicit solvent methods, which was developed on the base of liquid-state theory. The RISM includes a reasonable level of solvent structure treatment by rigorous statistical-mechanics description and, thus, overcomes shortcomings of explicit solvent methods. Here, we provide with main equations of the RISM, while its detailed description can be found elsewhere.[2-4] We employed 3-dimensional version of RISM (3D-RISM), where a solute molecule is modeled as a single object, while solvent molecules are represented as a set of atoms – sites (Figure S1).

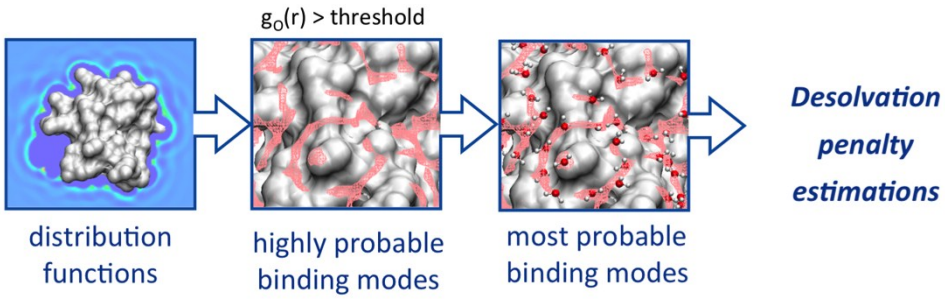

Scheme S1. General workflow for predictions of explicit water molecules' positions

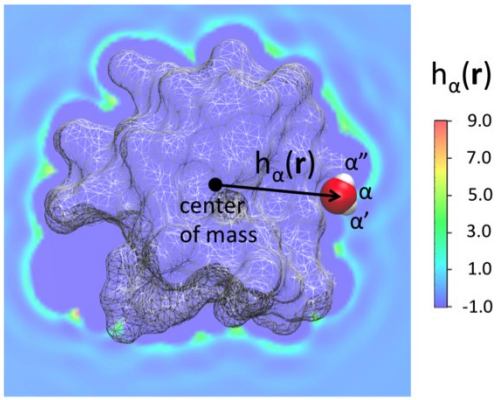

Figure S1. 3D intermolecular solvent site - solute correlation function $h_\alpha(\mathbf{r})$ around a model solute, where index α corresponds to the solvent sites.

The 3D-RISM equation relate 3D intermolecular solvent-site – solute correlation functions:

$$h_\alpha(\mathbf{r}) = \sum_{\alpha=1}^{N} \int_{R^3} c_\alpha(r - r') \chi_{\alpha\alpha'}(|r'|) dr' \qquad \text{(Eq. S1)}$$

Here, $h_\alpha(r)$ and $c_\alpha(r)$ are the total and direct correlation functions (index α corresponds to the solvent sites), $\chi_{\alpha\alpha'}(r)$ is the bulk solvent susceptibility function, and N is the number of sites in a solvent molecule. The solvent susceptibility function describes the mutual correlations in the bulk solvent. It can be obtained from the corresponding site-site total correlation functions and the solvent number density (ρ_α):

$$\chi_{\alpha\alpha'}(r) = w^{solv}_{\alpha\alpha'}(r) + \rho_\alpha h^{solv}_{\alpha\alpha'}(r) \qquad \text{(Eq. S2)}$$

where $\omega_{\alpha\alpha'}{}^{solv}(r)$ is the intramolecular correlation function, which describes molecular structure of a single solute molecule:

$$w_{\alpha\alpha'}(r) = \frac{\delta(r-r')}{4\pi r^2_{\alpha\alpha'}} \qquad \text{(Eq. S3)}$$

While site-site total correlation functions, $h_{\alpha\alpha'}{}^{solv}(r)$, are obtained via solvation of 1D-RISM equations (see reference 2 for details).

To make Eq. S1 complete, closure relations are introduced:

$$h_\alpha(\mathbf{r}) = \exp\left[-\beta u_\alpha(\mathbf{r}) + h_\alpha(\mathbf{r}) - c_\alpha(\mathbf{r}) + B_\alpha(\mathbf{r})\right], \qquad \text{(Eq. S4)}$$

where $u_\alpha(\mathbf{r})$ is the interaction potential between the solute molecule and site of solvent, $B_\alpha(\mathbf{r})$ is the bridge functional, $\beta = 1/k_BT$, k_B is the Boltzmann constant, and T is the temperature. The exact bridge functions in Eq. S4 are represented as an infinite series of integrals over high order correlation functions and are, therefore, practically incomputable, which makes it necessary to incorporate some approximations. In the current work, we use a closure relationship proposed by Kovalenko and Hirata (the KH closure),[5] which was designed to improve convergence rates and to prevent possible divergence of the numerical solution of the RISM equations:

$$h_\alpha(\mathbf{r}) = \begin{cases} \exp\left[\Xi_\alpha(\mathbf{r})\right] - 1 & \text{when } \Xi_\alpha(\mathbf{r}) < 0 \\ \Xi_\alpha(\mathbf{r}) & \text{when } \Xi_\alpha(\mathbf{r}) > 0 \end{cases} \qquad \text{(Eq. S5)}$$
$$\Xi_\alpha(\mathbf{r}) = -\beta u_\alpha(\mathbf{r}) + h_\alpha(\mathbf{r}) - c_\alpha(\mathbf{r})$$

1.1.2. 3D-RISM calculations with MOE software[6]

- **X-ray structures pre-processing** was performed using *QuickPrep* utility with default parameters apart of Refine step (Figure S2).

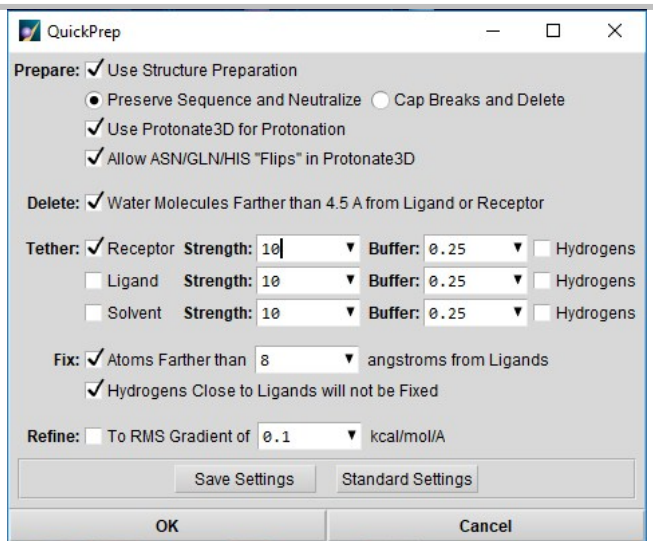

Figure S2. QuickPrep parameters employed in the study

- **3D-RISM calculations** were performed using *Solvent Analysis* utility (Figure S3). The 3D grid around a solute was generated such that the minimum distance between any solute atom and the edge of solvent box (Buffer in MOE notation) was equal to 15 Å. The linear grid spacing in each of the three directions was 0.3 Å. We employed the MDIIS iterative scheme with default parameters (5 MDIIS vectors) and tight convergence.

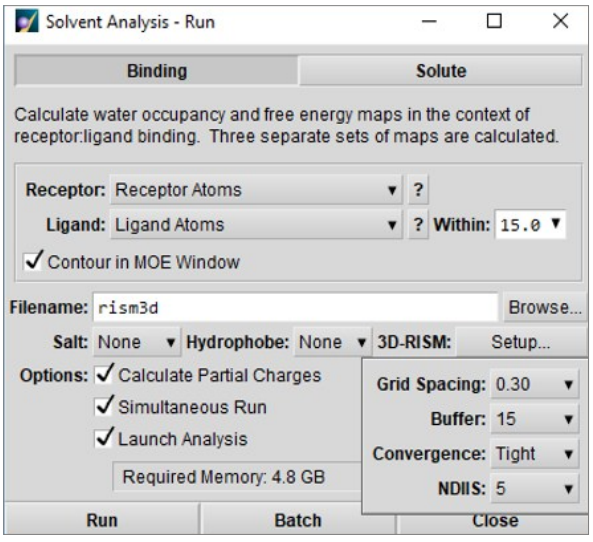

Figure S3. Solvent Analysis parameters employed in the study

- **Solvent Analysis results** are summed up in the correspond MOE panel (Figure S4-a). It contains data for all components of the system: protein, ligand, and their complex. In the study we employed the following in silico parameters for solvent analysis:

- *geometrical*: radial distribution functions, RDFs. The function gives a probability to find a water molecule at particular distance from a solute. They are closely connected to total correlation functions (FigureS1) as following:

$$h(r) = g(r) - 1 \qquad \text{(Eq. S6)}$$

They could be visualized using the correspondent Solvent Analysis - Grids panel (Figure S4-b,c). In the study we used only RDF of water oxygen atom with the cut-off g(**r**) >3.

- *geometrical*: explicit water positions defined from RDFs. They can be visualized using Create Water utility on the Solvent Analysis – sites panel (Figure S4-a)

- *energetical*: free energy maps. They contain information on a desolvation energy (free energy change accompaning a water transfer from a position around solute to a bulk solvent). They can be visualized in a similar way as RDFs (Figure S4-b,d). In the study we used only $\Delta G < 0$ with the cut-off $\Delta G_{des} < -5.0$ kcal/mol.

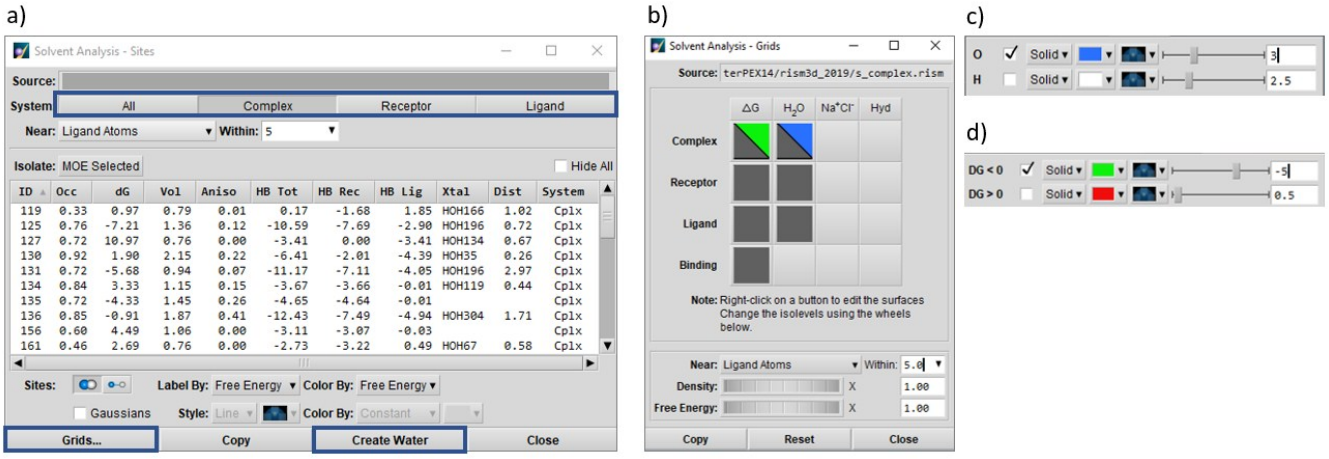

Figure S4. Results panel of Solvent Analysis in MOE software

1.1.3. Docking study with MOE software[6]

For compounds lacking X-ray structures in retrospective study (**8** and **9**) as well as for systems in prospective study (**10**) we performed docking using template-docking protocol implemented in MOE software (Figure S5). Molecules were docked in PEX14 crystal structure with PDB ID = 5L8A (complex with compound **2**), where the original ligand served as a sub-structure template. We employed rigid-receptor docking with default parameters.

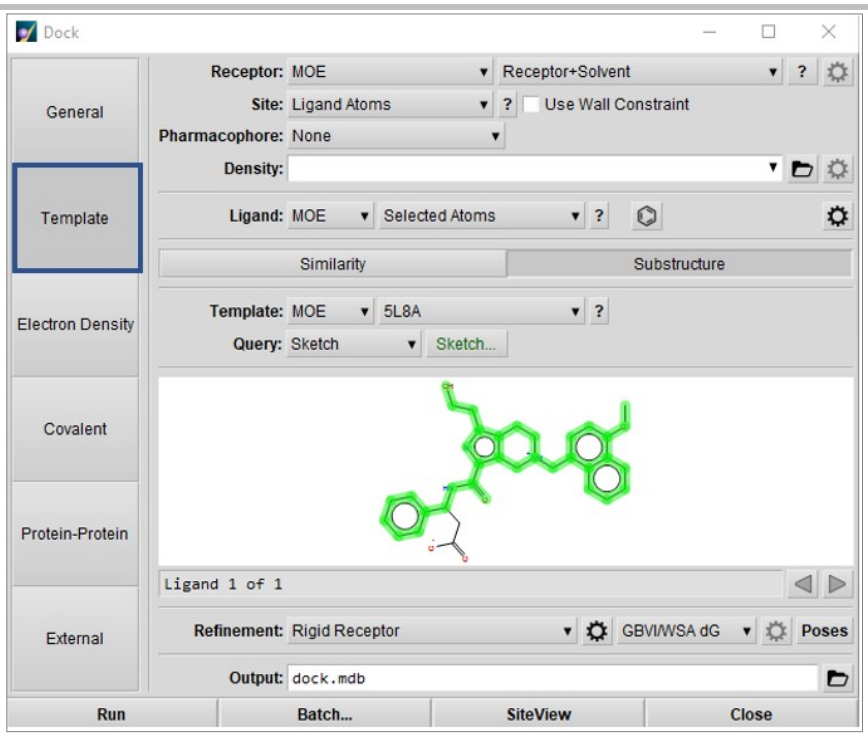

Figure S5. Template docking employed in the study

1.2. Experimental procedures

1.2.1. Crystallographic data preparation

Complexes of the N-terminal domain of PEX14 from *Trypanosoma brucei* with S3 and R3 were prepared by mixing a 10-fold molar excess of the ligand (50mM) dissolved in DMSO and the diluted protein (1mg/ml) in 10mM Tris pH 8 containing 100mM NaCl and 5mM β-mercaptoethanol. The mixture was incubated for 1h at room temperature. The complex was washed with fresh buffer using 10 kDa-cutoff Centricon to remove the DMSO and concentrated to about 30 mg/ml. Initial crystallization trials were set up using commercial kits in an automated mode. The initial crystals were optimized and diffraction quality crystals of the PEX14-S3 complex were obtained at room temperature in 0.2M Na_2SO_4, 0.1 M Bis-Tris propane pH 7.5, 20% (w/v) PEG 3350 while those of tbPEX14-R3 complex at 4°C in 0.22M Lithium Sulfate, 0.1M Tris-HCl pH 8.5, 29% PEG 4000. Crystals were cryo-protected in 25% (v/v) glycerol in the mother liquor and cryo-cooled in liquid nitrogen. The diffraction data for tbPEX14-S3 and tbPEX14-R3 crystals were collected at DESY (Hamburg, Germany) beamline P11. The experimental data were indexed, integrated and scaled using XDS and XSCALE software.[7] The Matthews coefficient was analyzed to estimate the number of molecules in the asymmetric unit.[8] Molecular replacement solution was found using Phaser[9] with tbPEX14 structure (PDB code: 5AON[10]) as a search model. The electron densities describing the ligands were perfectly visible prior to the introduction of the inhibitor molecules into the model. The high resolution data allowed for unambiguous placement of the inhibitors. The models were built and the inhibitors were placed using

COOT,[11] followed by iterations of Refmac5 refinement[12] and manual rebuilding. Throughout the refinement 5% of the reflections were used for cross-validation analysis,[13] and the behavior of R_{free} was employed to monitor the refinement strategy. Water molecules were added using Arp/Warp[14] and subsequently manually inspected. The data collection and refinement statistics are summarized in Table SI-1.

Table SI-1: Data collection and refinement statistics. Statistics for the highest shell are listed in parentheses.

PDB ID	5OML	6RT2
Inhibitor	**10** *S*-isomer	**10** *R*-isomer
Data collection		
Space group	P 2 21 2	P 2 21 2
Cell constants:		
a, b, c (Å)	35.78, 115.52, 38.87	35.86, 116.37, 38.96
α, β, γ (°)	90.00, 101.39, 90.00	90.00, 101.46, 90.00
Wavelength (Å)	1.000	1.033
B factor (Wilson) (Å 2)	23.44	29.40
Resolution range (Å) (highest shell)	38.51 - 1.30 (1.35-1.30)	58.2 – 1.50 (1.54-1.50)
Completeness (%)	96.8 (98.4)	95.6 (88.9)
Rmerge (%)	2.8 (46.8)	5.3 (72.8)
Rmeas (%)	3.5 (57.7)	6.7 (92.6)
Observed reflections	365510(38185)	236503(15944)
Unique reflections	145521(15874)	94579 (6429)
I/σ(I)	14.55 (1.81)	9.04 (1.33)
Redundancy	2.50 (2.40)	2.50 (2.48)
Refinement		
Resolution (Å)	20.0 – 1.30	25.0 - 1.50
Number of reflections used	71864	46462
R-factor (%)	16.4	17.7
Rfree (%)	19.1	20.2
Average B (Å 2)		
Protein	15.3	24.4
Ligand	18.8	24.5
Water	30.8	34.0
RMS from ideal values		
Bond length (Å)	0.036	0.026
Bond angles (°)	3.0	2.4
Ramachandran statistics (%)		
Most favored regions	97.9	97.5
Additionally allowed regions	2.1	2.5
Generously allowed regions	0.0	0.0
Content of asymmetric unit		
Number of protein molecules/residues/atoms	4/66/2319	4/66/2213
Number of ligand molecules/atoms	4/156	4/156
Number of solvent molecules	512	403

1.2.2. AlphaScreen-based competition assay

To measure compounds half maximal inhibitory concentration (IC_{50}) values against PEX14-PEX5 interaction, an AlphaScreen-based assay was developed according to PerkinElmer indication. The assay mixture was composed of 3 nM N-His-PEX14 and 10 nM of biotinylated PEX5-derived peptide (ALSENWAQEFLA) in a PBS buffer supplemented with 5mg/mL of BSA and 0.01% (v/v) Tween-80. The assay employed 5 µg/mL of streptavidin donor beads and 5 µg/mL of nickel chelate acceptor beads (purchased from PerkinElmer). Each compound was added to the assay mixture as a DMSO solution. DMSO concentration was kept constant at 5% (v/v). This amount of DMSO was proven to have no effect on the assay readout.

The competition curves were measured using a serial dilution of the inhibitor while the concentrations of all other assay components were kept constant. Assay readings for each point were measured in quadruplicates and averaged. The inhibitor IC_{50} was calculated from the Hill sigmoidal fit of the experimental data with top asymptote fixed at maximal assay signal (no inhibitor added) and bottom asymptote set at 0, using OriginPro 9.4. In the cases where limited compound solubility prevented the AlphaScreen signal to drop to 0 despite the higher inhibitor concentration, such points were removed from the Hill sigmoidal fit calculation.

The curves for compounds **2** and **10** are shown on Figure S6, the experimental details for screening of other compounds are presented elsewhere.[15]

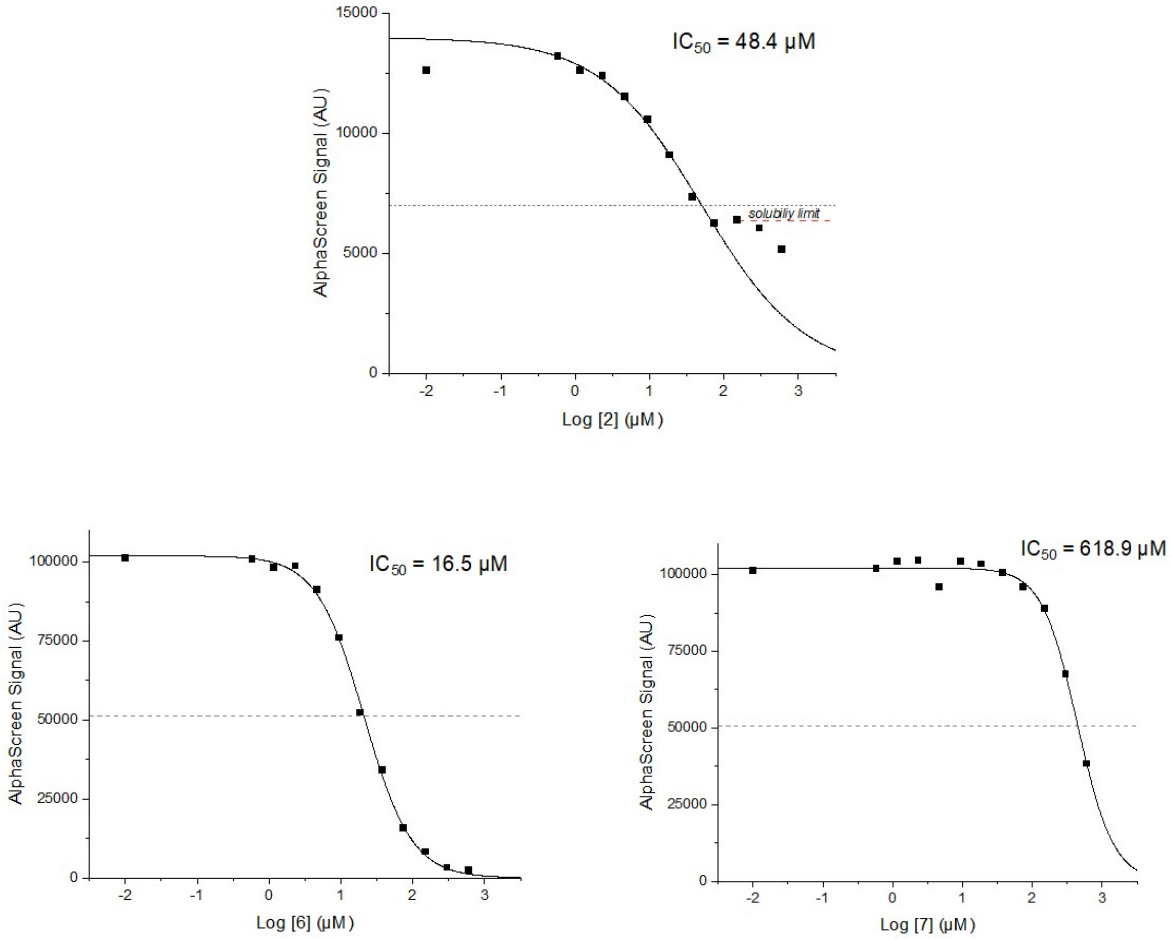

Figure S6. Competition of compounds **2** and **10** (*S*- and *R*-isomers) for the TbPEX14 N-terminal domain binding site are measured by an AlphaScreen assay. Each point of the curve is averaged on 4-points measurements, experimental error omitted for clarity.

1.2.3. Determination of the K_d by microscale thermophoresis (MST)

For the MST experiments, purified, His-tagged, *Trypanosoma brucei* PEX14 (tbPEX14) was labeled with Ni-NTA-ATTO647 (molar ratio 2:1) for 30 min at the room temperature. Labeled tbPEX14 was used at the final concentration of ~ 50nM. Serial dilutions of compound **10** (S- and R-isomers) (120nM-4 mM) were prepared in a 50mM Tris-HCl pH 7.4 containing 150mM NaCl, 10mM MgCl2 and 0.05 (v/v) % Tween-20 and the protein. The measurements were performed at 25°C on a NanoTemper Monolith NT.115 instrument using 40% light-emitting diode (LED) and 40% MST power. K_d values were calculated using MO.Affinity analysis software. The experiments were performed in triplicate.

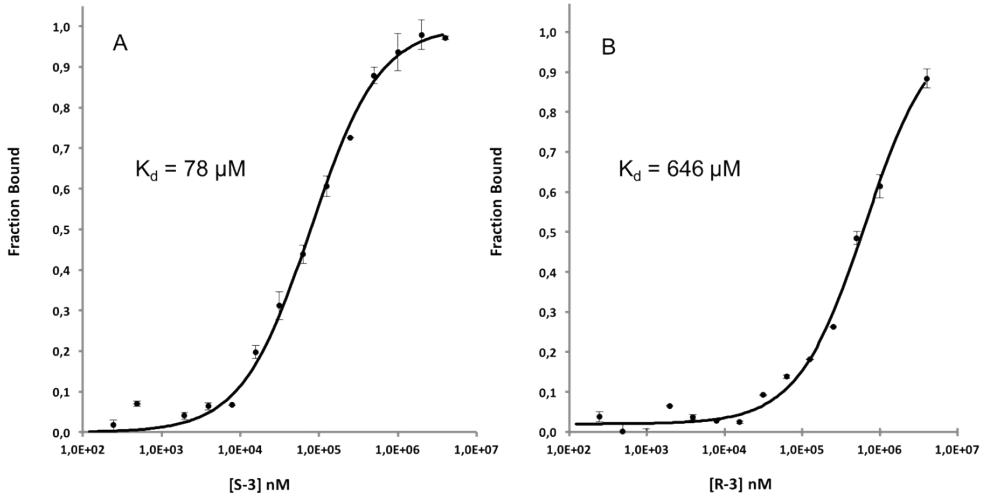

Figure S7. MST titration of tbPEX14. Dose-response curves for the binding interactions between Ni-NTA-ATTO647 labelled His6-tbPEX14 and compound **10:** (A) S-isomer; (B) R-isomer. The error bars represent the standard error of n=3 measurements.

2. Results and Discussion

2.1. Comparison of predicted water positions with X-ray data

For PEX14 structures we revealed an excellent agreement between predicted water positions and high-resolution X-ray data: PDB ID = 5L87; res. = 0.87Å (Figure S9).

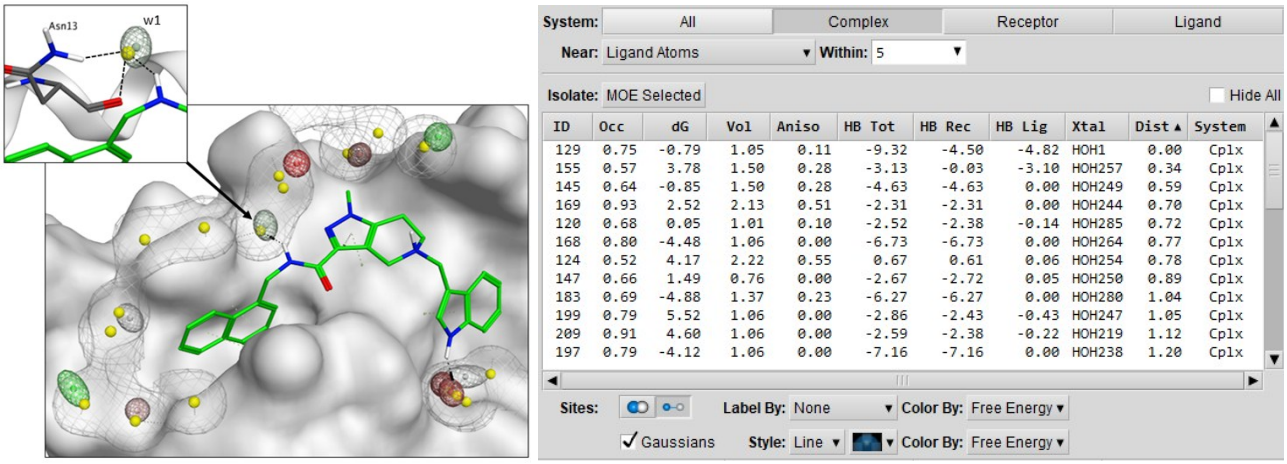

ID	Occ	dG	Vol	Aniso	HB Tot	HB Rec	HB Lig	Xtal	Dist ▲	System
129	0.75	-0.79	1.05	0.11	-9.32	-4.50	-4.82	HOH1	0.00	Cplx
155	0.57	3.78	1.50	0.28	-3.13	-0.03	-3.10	HOH257	0.34	Cplx
145	0.64	-0.85	1.50	0.28	-4.63	-4.63	0.00	HOH249	0.59	Cplx
169	0.93	2.52	2.13	0.51	-2.31	-2.31	0.00	HOH244	0.70	Cplx
120	0.68	0.05	1.01	0.10	-2.52	-2.38	-0.14	HOH285	0.72	Cplx
168	0.80	-4.48	1.06	0.00	-6.73	-6.73	0.00	HOH264	0.77	Cplx
124	0.52	4.17	2.22	0.55	0.67	0.61	0.06	HOH254	0.78	Cplx
147	0.66	1.49	0.76	0.00	-2.67	-2.72	0.05	HOH250	0.89	Cplx
183	0.69	-4.88	1.37	0.23	-6.27	-6.27	0.00	HOH280	1.04	Cplx
199	0.79	5.52	1.06	0.00	-2.86	-2.43	-0.43	HOH247	1.05	Cplx
209	0.91	4.60	1.06	0.00	-2.59	-2.38	-0.22	HOH219	1.12	Cplx
197	0.79	-4.12	1.06	0.00	-7.16	-7.16	0.00	HOH238	1.20	Cplx

Figure S8. Left: Water-mediated interactions between ligand and polar receptor residues in complex PDB ID = 5L87 (inserted subfigure – position of the most energetically-favourable water molecule, w1). Crystallographic water positions are shown with yellow spheres and their vdW volume is shown with a grey-netted surface, while predicted water positions are shown with a netted sphere reflecting entropy of the molecule and coloured with respect to ΔG_{des} ('happy' = green, 'unhappy' = red). Right: Energetic and structural parameters for predicted water positions: ID is the molecule number, dG is the desolvation free energy, Dist is the distance to the closest experimentally defined position of water (Xtal).

2.2. SAR in HS_1 pocket

We observed that binding to the cavity HS_1 is purely lipophilicity-driven (chemistry on R_1-group is shown in Figure SI-1). The most pronounced change in affinity, ca. 1 log-unit, is associated with growing of phenyl ring to naphthyl one. IC50 values and corresponding curves for the compounds will are reported elsewhere.[15]

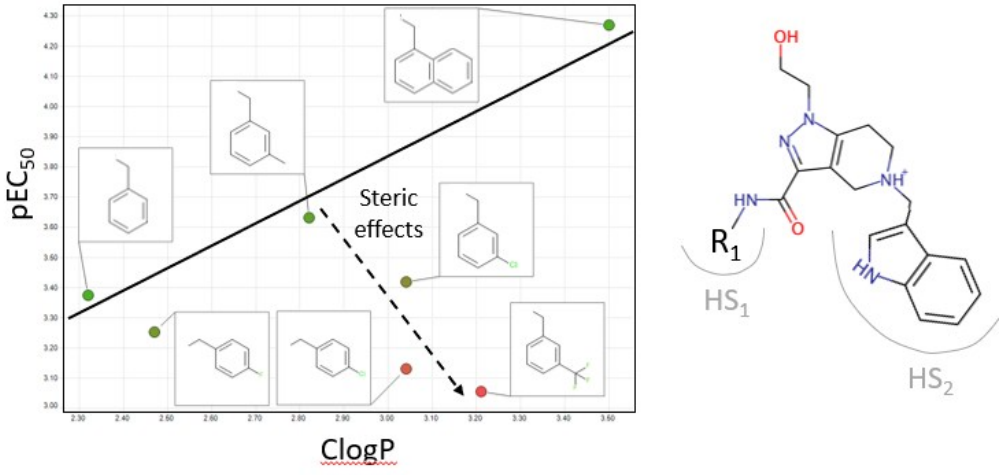

Figure S9. SAR on R_1-group of the inhibitors, data points are coloured with respect to LLE = pIC50 - clogP (min = red, max = green). Dashed line indicated dpot in potency due to clashes with the receptor.

2.3. Solvent analysis of the HS_2 cavity

Solvent analysis of the HS_2 cavity revealed that water patterns are different for indole and naphthyl rings (Figure S10). Upon binding of the indole ring, one water molecule from the ligand's solvation shell (w1) remained bound and formed connections with two water molecules remaining in the cavity (w2 and w3) (Figure S10 a,b). In contrast, the methoxynaphthyl moiety efficiently displaced all water molecules from the HS_2 cavity (Figure S10 c,d). For two extreme cases of reduced-potency compounds **8** and **9**, where it was not experimentally possible to obtain X-ray structures, we performed a docking study. Binding of the corresponding molecules were investigated for both configurations of the HS_2 cavity (Figure 2, *bottom*). Since water molecules remained in the cavity after binding in both cases, the most probable conformation of Thr^{22} residue was the one stabilizing the water network in the cavity (Figure S10 e,f). In case of compound **8**, loss of potency was due to the presence of very energetically-unfavorable water in the cavity (w2), which came together with the ligand as a part of its solvation shell but was pushed deeply into the lipophilic pocket than w1 for inhibitor containing the indole ring (Figure S10 a). In turn, the naphthyl group of compound **9** does not approach sufficiently into the pocket to

efficiently displace all water molecules from the cavity, which also resulted in the presence of very energetically-unfavorable water molecules.

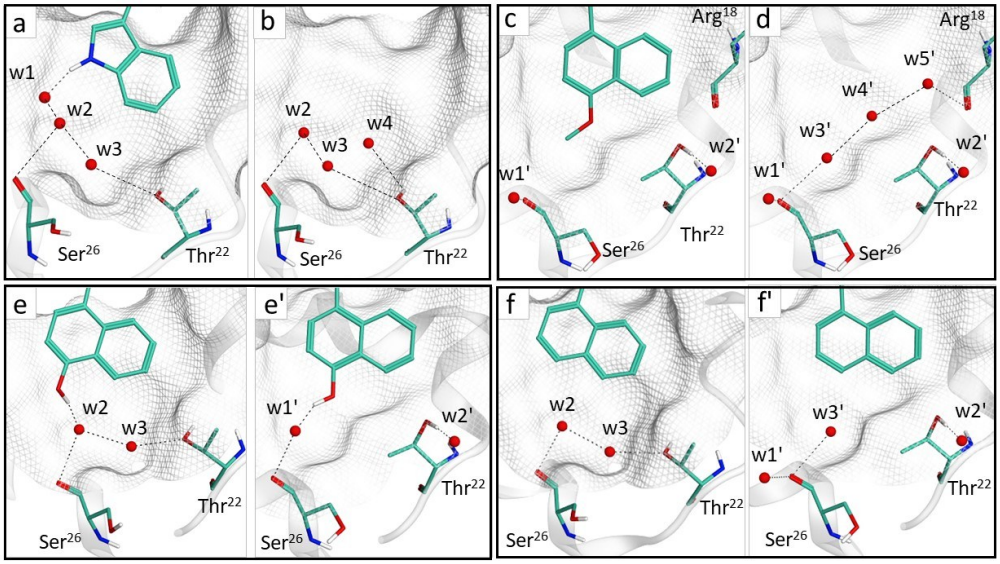

Figure S10. Water analysis in the hot-spot HS_2 cavity. ***Top*:** Predicted positions of water molecules in X-ray structures for two types of R_2-group: (a) complex with inhibitor containing the indole ring (PDB ID = 5L87), (b) the same, ligand-free cavity, (c) complex with inhibitor **2** containing methoxynaphthyl moiety (PDB ID = 5L8A), and (d) showed the corresponding ligand-free cavities, which are different in shape due to change in conformation of Thr^{22}. ***Bottom*:** Simulated binding poses of compounds **8** (e, e') and **9** (f, f') for both configurations of HS_2 cavity.

2.4. Population of *cis*- and *trans*-isomers of inhibitor in the crystal structure PDB ID = 5L8A

In crustal structure PDB ID = 5L8A one observed 3:1 ratio of *cis*- to *trans*-isomers, which can be explained by the Boltzmann distribution of the population of the two isomeric states, which is tightly dependent on temperature:

- At room temperature the *cis*- and *trans*-isomers can be formally considered as conformers, and the energy required for the tautomerization is relatively low. So, the two forms can coexist, with the trans- isomer slightly more populated due to the lower energy.
- At lower temperatures (as in frozen crystal), the things are, however, different. While the energy barrier for the interconversion will not change, the thermal motion of the molecules will be consistently lower, and it could be that the cis-isomer's energy will become lower due to the desolvation contribution.

Unfortunately, it was not possible to experimentally confirm the isomerization of the compound in solution as its solubility did not allowed for reliable NMR spectra acquisition. Instead, we performed molecular dynamics (MD) simulations of the *cis*- and *trans*-isomers extracted from the corresponding crystallographic unit (respectively molecule D and molecule A), both ligand in solution and in complex with PEX14.

Table SI-2: Technical data of Molecular dynamics simulations.

Parameter	Characteristics
Force Field	AMBER14, minimized after solvation (1000 steps, simulated annealing)
Solvent model	TIP3P, preserved crystallographic waters
Total simulation time	50 ns
Snapshot interval	100 ps, total steps: 501
Cutoff for long-range forces	8Å
Criteria for solvation assessment (solvent model waters):	0 if distance >3Å from carbonyl oxygen of the ASN13 backbone 1 if distance <3Å from carbonyl oxygen of the ASN13 backbone

According to molecular dynamics (MD) simulations:

- Both isomers coexist in solution and each of them can interact with the binding site of PEX14.
- The isomerization between the two forms is an event that happens only in solution, not when the compound is bound to the protein (the position of the benzyl moiety attached to the amide nitrogen is frozen due to hydrophobic contacts with the binding site).
- Due to the geometry of the amide bond in the *cis*-isomer complex, the stabilization effect on the "happy" water is highly impaired. The water pocket created by the backbone of Asn[13] residue and the pyrazole moiety of the compound is empty for 84% of the simulation time (see figures below). Therefore, for the cis-isomer complex, the presence of "happy" water is a crystallographic artifact as it does not contribute to binding
- Overall solvation environment of the cis-isomer complex is consistently different from that of the trans-isomer complex.

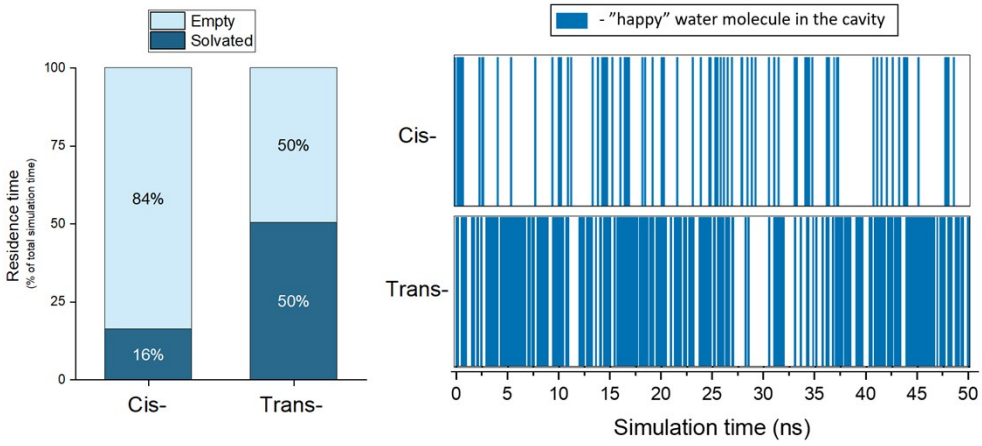

Figure S11. MD results on "happy" water residence time in PEX14 complex with cis- and trans- isomers of the inhibitor

However, due to the following reasons we consider the observed *cis*-isoform as a crystallization artifact:

- [As discussed in the main body of the manuscript] Our attempts to remove the "happy" water connected to Asn[13] by medicinal chemistry modification of the ligand has been unsuccessful.[15] This indicates that the contacts formed between trans-isomer and the "happy" water are essential for the binding. This, in turn means that *trans*-isomer is the one important for binding.
- Structures with both *trans*- and *cis*-isomers being present only in one crystal structure (PDB ID = 5L8A) and we did not observe *cis*-isomer in any other structure of PEX14 solved so far (e.g. crystal structure PDB ID = 6SPT of PEX14 complex with structurally close ligand, were only trans-isomer of the inhibitor was observed). We have also two unpublished structures (due to IP protection) that are in trans-configuration.

Author Contributions

ELR – writing of the manuscript (lead), RISM calculations and solvent analysis (lead), funding acquisition (supporting)

MD – study design (supporting) and synthesis of the compounds (lead)

VN - crystallographic and affinity study (equal)

GD - crystallographic and affinity study (equal), manuscript preparation (supporting)

RF - molecular dynamics analysis (lead), pocket analysis (supporting)

MSO - Alpha Screen measurements (lead)

MS – project lead (equal), analysis (supporting), writing of the manuscript (supporting)

GP – project lead (equal), manuscript preparation (equal), crystallographic data analysis (lead), study design and execution (lead)

IVT - study design (supporting), manuscript preparation (supporting), project lead (equal)

References

1. L. S. Ornstein and F. Zernike, *Koninklijke Nederlandse Akademie van Wetenschappen Proceedings Series B Physical Sciences*, 1914, **17**, 793-806.
2. J.-P. Hansen and I. R. McDonald, *Theory of simple liquids : with applications of soft matter*, Elsevier/AP, Amstersdam, Fourth edition. edn., 2013.
3. D. Chandler and H. C. Andersen, *J. Chem. Phys.*, 1972, **57**, 1930-1937.
4. D. Beglov and B. Roux, *J. Phys. Chem. B*, 1997, **101**, 7821-7826.
5. A. Kovalenko and F. Hirata, *J. Chem. Phys.*, 1999, **110**, 10095-10112.
6. MOE, Molecular Operating Environment (MOE), http://www.chemcomp.com/Products.htm).
7. W. Kabsch, *Acta Crystallogr D Biol Crystallogr*, 2010, **66**, 133-144.
8. K. A. Kantardjieff and B. Rupp, *Protein Sci*, 2003, **12**, 1865-1871.
9. A. J. McCoy, R. W. Grosse-Kunstleve, P. D. Adams, M. D. Winn, L. C. Storoni and R. J. Read, *J Appl Crystallogr*, 2007, **40**, 658-674.
10. Y. Watanabe, K. Kawaguchi, N. Okuyama, Y. Sugawara, T. Obita, M. Mizuguchi, M. Morita and T. Imanaka, *FEBS Lett*, 2016, **590**, 242-250.
11. P. Emsley, B. Lohkamp, W. G. Scott and K. Cowtan, *Acta Crystallogr D Biol Crystallogr*, 2010, **66**, 486-501.
12. G. N. Murshudov, P. Skubak, A. A. Lebedev, N. S. Pannu, R. A. Steiner, R. A. Nicholls, M. D. Winn, F. Long and A. A. Vagin, *Acta Crystallogr D Biol Crystallogr*, 2011, **67**, 355-367.
13. A. T. Brunger, *Nature*, 1992, **355**, 472-475.
14. R. J. Morris, A. Perrakis and V. S. Lamzin, *Methods Enzymol*, 2003, **374**, 229-244.
15. M. Dawidowski, V. C. Kalel, V. Napolitano, R. Fino, K. Schorpp, L. Emmanouilidis, D. Lenhart, M. Ostertag, M. Kaiser, M. Kolonko, B. Tippler, W. Schliebs, G. Dubin, P. Maser, I. V. Tetko, K. Hadian, O. Plettenburg, R. Erdmann, M. Sattler and G. M. Popowicz, *J. Med. Chem.*, 2020, **63**, 847-879.